*J. Fluid Mech.* (1985), *vol.* 154, *pp.* 321–336
*Printed in Great Britain*



# Effect of rotation on isotropic turbulence: computation and modelling

By JORGE BARDINA†, J. H. FERZIGER
Department of Mechanical Engineering, Stanford University, Stanford, CA

AND R. S. ROGALLO
NASA–Ames Research Center, Moffett Field, CA

(Received 30 December 1983 and in revised form 30 November 1984)

This paper uses numerical simulation to analyse the effects of uniform rotation on homogeneous turbulence. Both large-eddy and full simulations were made. The results indicate that the predominant effect of rotation is to decrease the rate of dissipation of the turbulence and increase the lengthscales, especially those along the axis of rotation. These effects are a consequence of the reduction, due to the generation of inertial waves, of the net energy transfer from large eddies to small ones. Experiments are also influenced by a more complicated interaction between the rotation and the wakes of the turbulence-generating grid which modifies the nominal initial conditions in the experiment. The latter effect is accounted for in simulations by modifying the initial conditions. Finally, a two-equation model is proposed that accounts for the effects of rotation and is able to reproduce the experimental decay of the turbulent kinetic energy.

## 1. Introduction

Rotation is known to have profound effects in fluid mechanics. Geophysical flows are strongly influenced by the Earth's rotation, and shear flows (boundary layers, for example) are stabilized or destabilized by the introduction of rotation. The effects of rotation are described by Greenspan (1968), and in other texts.

Since turbulence is created by instability, it is strongly affected by system rotation. The effect of rotation on turbulence production is discussed in the papers of Johnston, Halleen & Lezius (1972), Ferziger & Shaanan (1976) and Tritton (1981). The effect of rotation on homogeneous isotropic turbulence, however, is more subtle and not well understood. There have been three experiments in this area, and the inferences therefrom differ with respect to the effect of the rotation on the decay of the turbulence.

The experiment by Traugott (1958) is similar in design to that of Wigeland & Nagib (1978) described below. For this reason and because only one case with rotation was presented by Traugott, we shall not discuss this experiment in detail. Traugott's primary conclusion is that rotation decreases the rate of decay of the turbulence, i.e. the turbulence decays more slowly in the presence of rotation.

Ibbetson & Tritton (1975) used a unique apparatus in which turbulence was produced by dropping a grid through a rotating chamber. They found that the turbulence decayed more rapidly when the apparatus was rotating than when it was not. In this experiment, the chamber was small and the measurements were made

† Present address: PEDA Corporation, Palo Alto, CA.

at relatively long time intervals. As a result, the walls of the chamber probably affected the decay of the turbulence, which should therefore not be regarded as homogeneous. In fact, Ibbetson & Tritton offered the interaction of the walls with inertial waves as the probable explanation of the observed change in the rate of decay of the turbulence. As this flow was not truly homogeneous, it cannot be used for the purposes of this paper.

The most recent experiment, by Wigeland & Nagib (1978), hereinafter referred to as WN, consisted of a uniform flow set into solid-body rotation as it passed through a rotating honeycomb and a rotating turbulence-generating grid. The decay of the resulting turbulence was then studied in a stationary test section.

The primary purpose of WN was to resolve the apparently contradictory conclusions of Traugott (1958) and Ibbetson & Tritton (1975). For this reason WN utilized a number of different flow conditions in which the flow speed, turbulence-generating grid and rotation rate were varied. The ranges of the principal parameters utilized in these experiments are shown in table 1. Reynolds and Rossby numbers based on both the mesh size (subscript M) and the turbulence lengthscale (subscript T) are presented.

The WN results show various effects of rotation. In most cases, the turbulence intensity decays more slowly and the time-integral scales increase more rapidly as the rotation rate is increased. In a few cases, the turbulence intensity decays faster at small rotation rates but slower at larger rates of rotation. In the latter cases, the time-integral scale for the normal (to $\boldsymbol{\Omega}$ the imposed angular velocity) components of the turbulent velocity shows no change relative to the case without rotation. The dominant effect of rotation is to decrease the rate of decay of the turbulence. The increasing rates of decay sometimes seen at low rotation rates appear to be a separate effect of rotation on the process of turbulence generation just downstream of the grid.

A number of other experiments on the interaction of turbulent flow with rotation have been performed. These are mainly related to applications in which inhomogeneity is an important feature of the flow (meteorological and oceanographic problems and turbomachinery) and are not of direct interest to us. Among these, however, the recent works of Hopfinger & Browand (1982) and Hopfinger, Browand & Gagne (1982) should be mentioned. They report an experiment performed in a rotating tank with an oscillating grid at the bottom. Since the grid produces turbulence only at the bottom of the tank, this experiment is quite inhomogeneous, but some of their observations will be referred to later in this paper.

The current state of the art in turbulence modelling is described in the Evaluation Committee Report of the 1980–81 AFOSR–HTTM–Stanford Conference on Complex Turbulent Flows (Kline, Cantwell & Lilley 1982), which states in part: 'The fact that none of the present methods is influenced by rotation of the turbulent flow is an indication that present models are deficient in this respect.' Turbulence models which take rotation into account have been proposed by Rodi (1979) and Launder, Priddin & Skarma (1977). Rodi's model contains a term proportional to the spatial gradient of the rotation rate and has no effect on flows in uniform rotation, which are considered here. The model proposed by Launder *et al.* (1977) is not well behaved at high rates of rotation (or streamline curvature) because the energy-dissipation rate can become negative.

As the effects of rotation on turbulence are both multifold and subtle, the development of models which account for the effects of rotation requires an understanding of the processes occurring in these flows. In this paper, we study homogeneous turbulence in uniform rotation; effects that occur only in the presence

| Parameter | Traugott (1958) | Ibbetson & Tritton (1975) | Wigeland & Nagib (1978) |
|---|---|---|---|
| Rotation rate $\Omega$ s$^{-1}$ | 210 | 1–6.4 | 6–80 |
| Downstream distance $x/M$ | 17.5–27.5 | 144–3600 | 20–180 |
| Time s | 0.008–0.014 | 4–100 | 0.005–0.083 |
| $Re_M = UM/\nu$ | 5500 | 1200 | 900–3800 |
| $Ro_M = U/\Omega M$ | 10 | 28–180 | 10–600 |
| $Re_T = (\frac{1}{3}Q^2)^{\frac{1}{2}}\lambda/\nu$ | 30 | $\sim 10$ | 9–18 |
| $Ro_T = (\frac{1}{3}Q^3)^{\frac{1}{2}}/\Omega\lambda$ | 1.65 | $\sim 4$ | 0.4–16 |

TABLE 1. Parameter range of experiments. $M$ is the mesh size of the turbulence-generating grid, $U$ the experimental mean velocity in the $z$-direction, $Q^2$ the turbulence intensity per unit mass, $\lambda$ the Taylor microscale and $\nu$ the kinematic viscosity.

of mean strain are excluded. The Reynolds-stress equations for a homogeneous flow in uniform rotation about the $x_3$-axis are, in a rotating coordinate frame:

$$\left.\begin{aligned}
\frac{1}{2}\frac{\mathrm{d}\langle u_1^2\rangle}{\mathrm{d}t} &= 2\Omega\langle u_1 u_2\rangle - \epsilon_{11} + \phi_{11};\\
\frac{1}{2}\frac{\mathrm{d}\langle u_2^2\rangle}{\mathrm{d}t} &= -2\Omega\langle u_1 u_2\rangle - \epsilon_{22} + \phi_{22};\\
\frac{1}{2}\frac{\mathrm{d}\langle u_3^2\rangle}{\mathrm{d}t} &= -\epsilon_{33} + \phi_{33};\\
\frac{\mathrm{d}\langle u_1 u_2\rangle}{\mathrm{d}t} &= 2\Omega(\langle u_2^2\rangle - \langle u_1^2\rangle) - \epsilon_{12} + \phi_{12};
\end{aligned}\right\} \tag{1}$$

where $\langle\ \rangle$ indicates an ensemble or time average, $u_i$ the component of the turbulence velocity in the $i$-direction and $\epsilon_{ij}$ and $\phi_{ij}$ are the components of the dissipation and pressure-strain tensors, respectively. For definitions of the latter, see Reynolds (1976).

When the first three of these equations are summed, the sums of the rotation and pressure-strain terms each vanish, and the resulting equation for the turbulence intensity ($Q^2 = \overline{u_1^2} + \overline{u_2^2} + \overline{u_3^2}$) shows no *direct* effect of rotation. Furthermore, if the turbulence is isotropic, the rotation and pressure-strain terms disappear individually from (1). Thus it appears that rotation merely redistributes energy among unequal Reynolds-stress components. Furthermore, rotation enters the equations for the components of the dissipation in a fashion almost identical with the way it enters the Reynolds-stress equations, so the effects we seek are not to be found in these equations either.

The effects of rotation are manifested through changes in the spectrum of the turbulence caused by nonlinear interactions; this has been shown explicitly by Bertoglio (1982). Greenspan (1968) made a linear analysis of the Fourier components of the velocity and showed that uniform rotation alters their phase but not their amplitude. Hence rotation has no direct effect on any quadratic statistical quantity, such as the Reynolds stress. However, rotation does affect odd moments of the turbulence velocity directly; this has also been shown by Aupoix, Cousteix & Liandrat (1983).

In the following sections, we present the results of numerical simulations of initially homogeneous isotropic turbulence in uniform rotation and show that is is possible

to duplicate the phenomena observed in the WN experiment. By taking advantage of the greater control over initial conditions that one has in computer simulations, we demonstrate that the increase in the decay rate at low rotational speeds found in some of WN's cases is due to interactions that occur in the initial region of the flow, and that the primary effect of rotation is indeed to decrease the rate of decay of the turbulence.

By further investigation of the results, we show that the Reynolds-stress tensor remains nearly isotropic in the presence of rotation and that the principal effect of rotation is to inhibit energy transfer to small scales resulting in increased turbulence lengthscales, particularly those in the direction of the axis of rotation. Finally, we offer a theoretical explanation of the effect and a simple model capable of predicting it.

## 2. Approach

We shall use numerical solutions of the Navier–Stokes equations as the basis for our work. In a frame rotating with constant angular velocity $\Omega$ about the $x_3$ axis, these equations (Greenspan 1968) are

$$\frac{\partial u_i}{\partial t}+\frac{\partial}{\partial x_j}(u_i u_j) = 2\epsilon_{ij3}\Omega u_j-\frac{\partial p}{\partial x_i}+\nu\frac{\partial^2 u_i}{\partial x_j\,\partial x_j}, \tag{2}$$

together with the continuity equation

$$\frac{\partial u_i}{\partial x_i}=0. \tag{3}$$

Equation (2) determines the evolution of the flow. The first term on the right-hand side of (2) represents the Coriolis force; the centrifugal force has been combined with the pressure gradient so that $p$ in (2) is the sum of the centrifugal potential and the static pressure divided by the density, i.e. $0.5(\boldsymbol{\Omega}\times\boldsymbol{r})\cdot(\boldsymbol{\Omega}\times\boldsymbol{r})+p_0/\rho$.

The initial velocity field is isotropic, homogeneous, divergence-free, and has a given energy spectrum, but is otherwise random.

Statistical homogeneity is replaced by strict periodicity in all three spatial directions, and Fourier (spectral) methods are used to compute all spatial derivatives. The reduced pressure is obtained as the solution of the Poisson equation that ensures continuity. The velocity field is advanced using a fourth-order Runge–Kutta method. All simulations were alias-free and were run on the NASA-Ames ILLIAC IV machine.

Two computational levels are used in this work. The first level is large-eddy simulation in which the large scales of motion (denoted by an overbar) are computed explicitly and the sub-grid scales are modelled by means of a simple eddy-viscosity model due to Smagorinsky (1963):

$$\tau_{ij}=(C_s\Delta)^2|\bar{S}|\bar{S}_{ij}, \tag{4}$$

where $\bar{S}_{ij}=\frac{1}{2}(\partial\bar{u}_i/\partial x_j+\partial\bar{u}_j/\partial x_i)$ is the strain rate of the large-scale field $\bar{u}_i$, $|\bar{S}|^2=2\bar{S}_{ij}\bar{S}_{ij}$, $\Delta$ is the filter width used in the calculation, $\tau_{ij}$ is the subgrid-scale Reynolds stress, and $C_s=0.21$ was obtained by fitting the decay of isotropic turbulence. For further details of large-eddy simulation, see Ferziger & Leslie (1979) or Ferziger (1981); a brief summary is given in the Appendix.

The initial energy spectrum for the large-eddy simulations was obtained by scaling the initial energy spectrum of Comte-Bellot & Corrsin (1971) such that the total energy and dissipation approximately match those of WN. The initial Reynolds

number based on Taylor microscale was approximately 15; the filter width was chosen so that $\epsilon_0 \Delta / Q_0^3 = 0.244$. The WN experiment exhibited a small anisotropy that was not modelled in the computation, so comparisons between the experiment and the computational results cannot be completely quantitative. Full (defiltered) turbulence quantities were calculated from these simulations using the method developed by Bardina, Ferziger & Reynolds (1980). Large-eddy simulation was used principally to investigate the effect of initial conditions and in matching the WN results; $16 \times 16 \times 16$ and $32 \times 32 \times 32$ grids were used.

The second approach was full simulation. In this method, the equations of motion (2) and (3) are solved directly, without filtering or averaging. Since this approach eliminates the uncertainty that arises from the use of a subgrid scale model and defiltering in large-eddy simulation, it is the preferred method for investigating the effects of rotation on turbulence in detail. For these simulations, the initial energy spectrum had a square shape and was allowed to decay until the velocity field approximated homogeneous isotropic turbulence; the resulting field was used as the initial condition for all rotation cases.

For further details of the large-eddy simulations, see Bardina (1983) and for details of the full simulations see Rogallo (1981).

## 3. Computational results

The first, exploratory, simulations were made with the large-eddy-simulation approach to determine the feasibility of using the method. It was found that large-eddy simulations with $16 \times 16 \times 16$ grids are incapable of following evolution of these flows, because the lengthscales grow rapidly and become constrained by the computational period in a time short compared to the observation period of WN.

Large-eddy simulations were run using a $32 \times 32 \times 32$ grid at various rotation rates; the parameters are given in table 2. The initial conditions for each case were matched to the corresponding WN case in the manner described above. It is important to point out again that in the WN experiment the initial conditions for each of the three rotation rates are not the same, although WN intended them to be so; the differences are important in understanding the results, as we shall show below. Figure 1 shows the decay of the turbulence intensity, together with the corresponding WN results. A striking similarity to the WN experimental results is apparent. At the small rotation rate, $\Omega = 20\ \mathrm{s}^{-1}$, the decay of the turbulence is faster than in the unrotated flow, while at the high rotation rate, $\Omega = 80\ \mathrm{s}^{-1}$, the decay of turbulence is slower than in the unrotated flow.

It is important to observe again that the initial turbulence intensity and dissipation rate are different in each one of WN's cases, including the ones presented above; in most cases, both intensity and dissipation rate increase with the rotation rate. As we shall demonstrate below, in the absence of any other effect of rotation, these variations in the initial conditions would produce a faster decay of the turbulence. On the other hand, we shall show below that the effect of rotation on initially isotropic turbulence decreases the rate of decay of the turbulence. At the lower rotation rate, the effect of the initial conditions may dominate and a faster decay rate will then be observed. At the higher rotation rates, the rotation effects dominate the effects of the initial conditions and the turbulence decays more slowly than in the case of no rotation.

Thus there are two mechanisms at work in these flows. In the initial region, the rotation influences the turbulence produced by the grid, increasing both the turbulence

| | | | | |
|---|---|---|---|---|
| Rotation rate $\Omega$ | $s^{-1}$ | 0 | 20 | 80 |
| Mean streamwise velocity $U_s$ | m/s | 5.3 | 5.45 | 5.7 |
| Mesh size $M$ | mm | 6.25 | 6.25 | 6.25 |
| Downstream distance $X/M$ | | 20–70 | 20–70 | 20–70 |
| Reynolds number $Re_T$ | | 17.4–15.1 | 15.9–13.8 | 18.0–16.0 |
| Rossby number $Ro_T$ | | $\infty$ | 6.3–1.2 | 1.4–0.4 |
| Initial turbulence intensity $U_s/Q$ | | 334.1 | 329.1 | 327.9 |
| Initial dissipation $\epsilon$ | $m^2/s^3$ | 2.60 | 3.58 | 3.38 |

TABLE 2. Experimental data for one Wigeland & Nagib (1978) data set

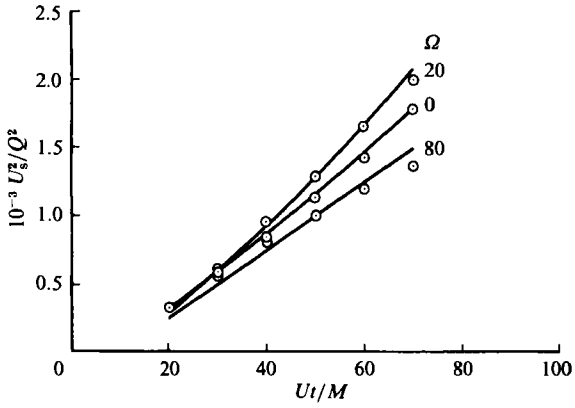


FIGURE 1. Results of large-eddy simulation compared to the experimental data of Wigeland & Nagib (1978). The initial energy and dissipation rate are matched to the experimental values. The grid was $32 \times 32 \times 32$, and the model constant $C_s = 0.21$.

intensity and dissipation rate at the initial experimental station just downstream of the grid. The exact mechanism that produces these effects is not understood at present, but it is probably connected with the stabilization/destabilization of shear flows by rotation.

In order to test the hypothesis that the effect of rotation on isotropic turbulence is to decrease the rate of dissipation, a further set of large-eddy simulations was made. Initial conditions identical with those used in the no-rotation case shown in figure 1 were used at all rotation rates. Figure 2 shows the time history of the decay of turbulence intensity with rotation rates of 0, 20, and 80 $s^{-1}$. The results support the hypothesis. Figure 3 shows that the average lengthscale of the energy-containing eddies, $l = Q^3/\epsilon$, grows more rapidly with increased rotation rate. Further details concerning the lengthscales are given below.

Full simulations were used to investigate the effects of rotation on the turbulence in more detail. In these cases, the turbulence was allowed to develop in the absence of rotation for some time. When the skewness of the velocity derivative reached its equilibrium value, the rotation was 'turned on'. This is an impossibility in the experiment, because it violates Helmholtz's theorem, but there is no reason why one cannot simulate it.

All full simulations reported here had the same isotropic initial conditions; the non-dimensional initial turbulence intensity was 4.88, the non-dimensional initial rate of energy dissipation was 16.78, and the initial Reynolds number based on the Taylor microscale was 17.4. The flow was allowed to decay until the non-dimensional

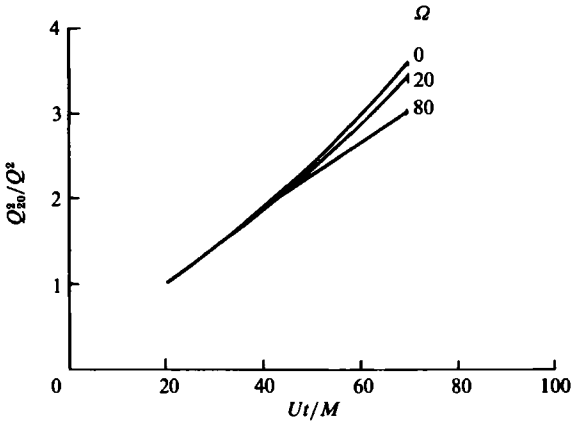


FIGURE 2. The decay of turbulence intensity in homogeneous rotating flows obtained by large-eddy simulation. All cases have the same initial conditions as the $\Omega = 0$ case shown in figure 1.

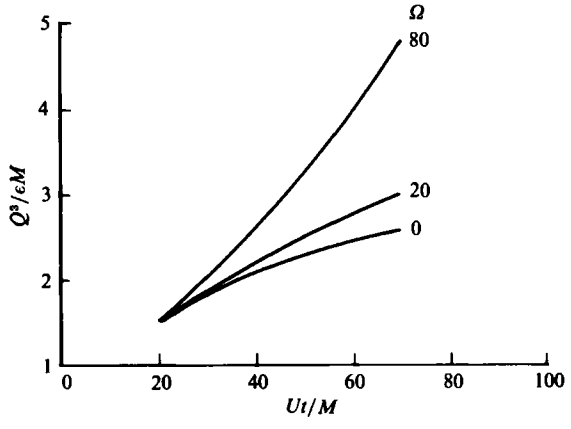


FIGURE 3. Growth of the average lengthscale in the homogeneous rotating flows of figure 2.

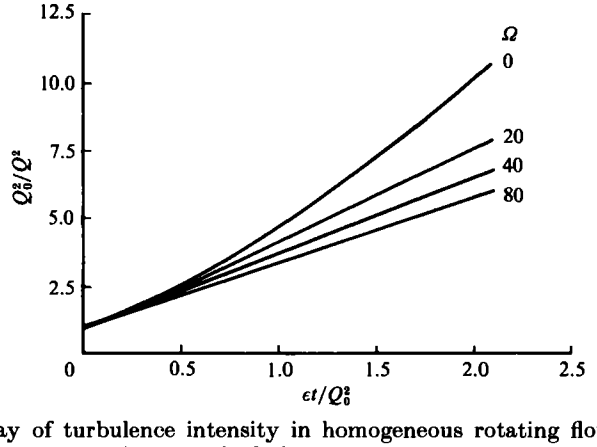


FIGURE 4. The decay of turbulence intensity in homogeneous rotating flows obtained by full simulation ($64 \times 64 \times 64$ grid). All cases had the same initial conditions and were run without rotation until $t = 0.3$.

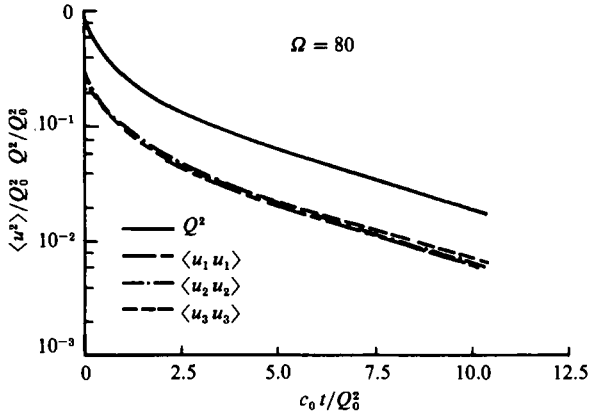


FIGURE 5. Time history of the components of the turbulence intensity in the $\Omega = 80\ \mathrm{s}^{-1}$ case of figure 4.

intensity became 1 before the rotation was turned on. Rotation rates of 0, 20, 40, and 80 $\mathrm{s}^{-1}$ were imposed on the flow. The ranges of Reynolds and Rossby numbers were 13–17 and 0.3–5.4, respectively. Figure 4 shows the time history of the decay of the turbulence intensity for rotation rates of 0, 20, 40, and 80 $\mathrm{s}^{-1}$. These results further confirm the hypothesis that rotation decreases the rate of decay of the turbulence.

One might expect rotation to produce anisotropy of the turbulence intensities. This is easily checked. As shown in figure 5, no significant differences among the components of the turbulence develop, but they appear to exchange small amounts of energy with each other. The exchange is not precisely periodic, but the timescale is approximately the inverse of the rotation rate; this could be anticipated from the Reynolds-stress equations (1).

We noted above that the lengthscales grow more rapidly when rotation is present, and one might expect them to become anisotropic. To investigate this, we computed the integral lengthscales:

$$\left.\begin{aligned} L_{ij,1} &= \int_0^{L_1} \frac{Q_{ij}(r_1,0,0)\,\mathrm{d}r_1}{Q^2}; \\ L_{ij,3} &= \int_0^{L_3} \frac{Q_{ij}(0,0,r_3)\,\mathrm{d}r_3}{Q^2}; \end{aligned}\right\} \tag{5}$$

where $Q_{ij}(r_1, r_2, r_3)$ is the two-point correlation function of the velocity components $u_i$ and $u_j$, and $Q^2$ is the turbulence intensity. The limits of integration should be infinite, of course, but in the simulation they were cut off at the point at which $Q_{ij}/Q^2 = 0.01$. The results for the no-rotation case are shown in figure 6. As expected, $L_{11,1} \simeq L_{33,3} \simeq 2L_{11,3} \simeq 2L_{33,1}$ in this case; all of these lengthscales appear to grow approximately linearly in time over the range studied. The results for $\Omega = 80\ \mathrm{s}^{-1}$ are shown in figure 7. All of the lengthscales have increased relative to the no-rotation case, but the most dramatic increases are in the lengthscales involving velocity components perpendicular to the rotation (3) axis. The largest increase is in $L_{11,3}$.

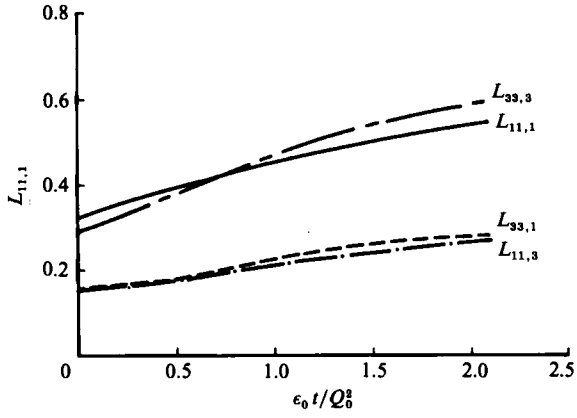


FIGURE 6. Growth of integral lengthscales in homogeneous isotropic turbulence (the $\Omega = 0$ case of figure 4).

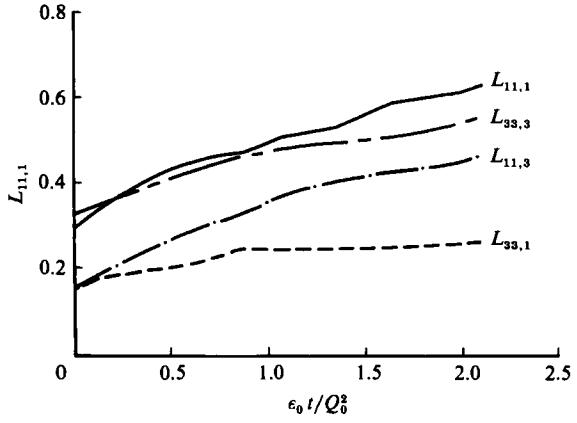


FIGURE 7. Growth of integral lengthscales in the $\Omega = 80\ \mathrm{s}^{-1}$ case of figure 4. The initial conditions are identical with those used to generate figure 6.

## 4. Physical interpretation

All of our simulations and the WN experiment were done at low Reynolds numbers. Extension of the results to higher Reynolds numbers must be done with caution.

The computational results demonstrate that rotation decreases the rate of energy dissipation of isotropic turbulence and increases the lengthscales. This suggests that the rotation interferes with the normal energy-cascade mechanism.

At low Rossby numbers $Q/\sqrt{3}\Omega L$, the motion tends to become essentially two-dimensional, in accord with the Taylor–Proudman theorem (Greenspan 1968). Hopfinger *et al.* (1982) observed a transition to an essentially two-dimensional state, which they called the quasi-geostrophic state, at $Ro \simeq 0.2$ (in our nomenclature). Since the WN flows and our simulations have Rossby numbers larger than this, we do not expect to observe this state. However, as already noted, we did observe a tendency for the lengthscales to increase more rapidly as the Rossby number is decreased. The growth of the lengthscales along the rotation axis is particularly rapid, indicating that the flow may be tending to the quasi-geostrophic state. No attempt to simulate the full transition was made, because, when the lengthscales become

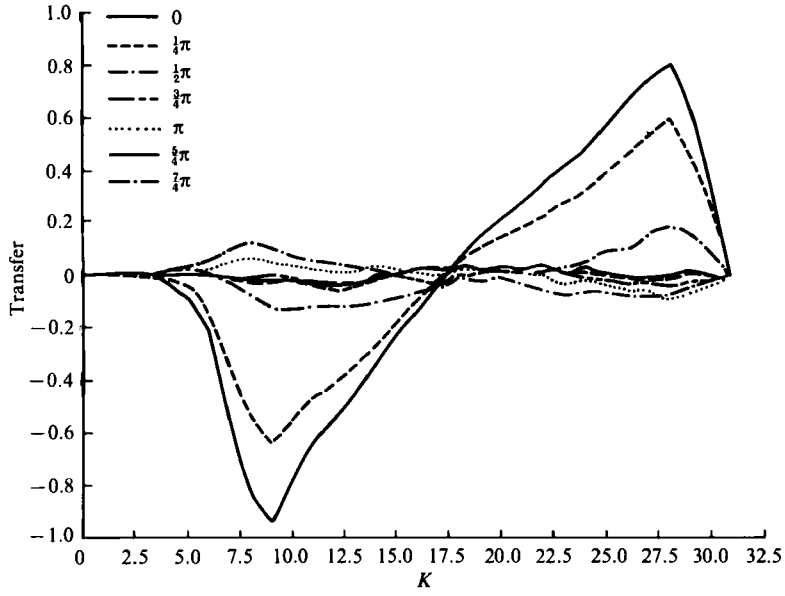


FIGURE 8. Energy transfer *vs.* wavenumber at zero Rossby number: the state at $t = 0$ is isotropic turbulence. The values shown in the legend are $2\Omega t$.

comparable to the size of the computational box, the validity of the numerical method is called into question and the results would be of dubious value. As Hopfinger *et al.* concentrated on the quasi-geostrophic region, their results cannot be compared with ours.

Although the large Rossby numbers used in the simulation render quantitative comparison with linear theory impossible, the latter may be used in a qualitative manner to explain some of the observed phenomena. In isotropic turbulence, the cascade process is a consequence of mutual deformation of randomly oriented vortex tubes. Rotation-induced Coriolis forces tend to align the vortex tubes with this axis; this is the essence of the Taylor–Proudman theorem. In doing so, rotation inhibits the cascading of energy to the smaller scales.

A more mathematical version of this argument can be constructed by noting that, for small Rossby numbers, Greenspan (1968) has shown that the velocity can be expressed as:

$$\boldsymbol{u}(\boldsymbol{k},t) = \boldsymbol{u}^{+}\left(\boldsymbol{k},\frac{qt}{L}\right)\mathrm{e}^{\mathrm{i}\omega t} + \boldsymbol{u}^{-}\left(\boldsymbol{k},\frac{qt}{L}\right)\mathrm{e}^{-\mathrm{i}\omega t}, \tag{6}$$

where $\omega(\boldsymbol{k}) = 2\Omega k_3/k$ ($\boldsymbol{k}$ being the wave vector) and $\boldsymbol{u}^{\pm}$ are amplitudes of the inertial waves. Equation (6) states that, in the limit of small Rossby number, the velocity field may be regarded as a superposition of inertial waves with characteristic frequency $\omega$ which are modulated on the longer turbulence timescale $L/q$. Cascading is an effect of the nonlinear terms in the Navier–Stokes equations; contributions to $\boldsymbol{u}(\boldsymbol{k})$ from products of $\boldsymbol{u}(\boldsymbol{k}')$ and $\boldsymbol{u}(\boldsymbol{k}'')$ are allowed only when $\boldsymbol{k} = \pm\boldsymbol{k}' \pm \boldsymbol{k}''$. As $Ro \to 0$, the contributing interactions are required to satisfy the additional resonant constraint:

$$\omega \pm \omega' \pm \omega'' = 0, \tag{7}$$

in order to transfer energy. At low Rossby numbers, this criterion is satisfied principally for small values of $k_3$, so we expect the nonlinear interactions to be limited to small $k_3$.

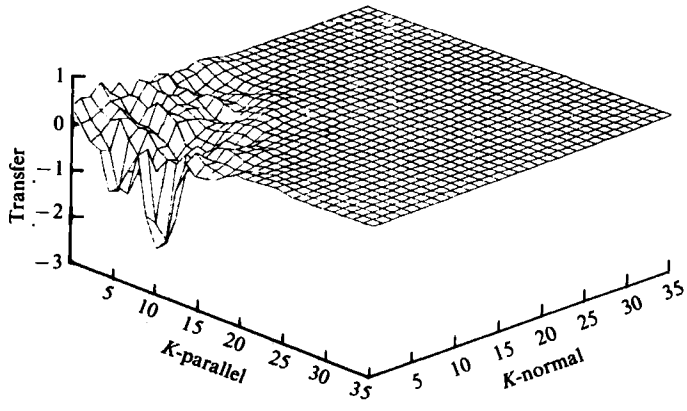


FIGURE 9. Distribution of energy transfer in wave space at $2\Omega t = \frac{1}{2}\pi$ of the flow shown in figure 8.

To illustrate these effects, we constructed a $Ro = 0$ simulation, by taking an isotropic turbulence field from a simulation and letting it evolve according to linear theory. Figure 8 shows the energy-transfer spectrum from this simulation. The energy transfer undergoes a rapidly damped oscillation in time. Its spectrum is not isotropic, however. Figure 9 shows the expected tendency of the transfer spectrum to become two-dimensional, i.e. to be concentrated near $k_3 = 0$. It is indeed surprising that the energy remains equally distributed among the three velocity components.

Bertoglio (1982) and Bertoglio & Mathieu (1983) have made simulations in which the nonlinear interactions were completely ignored, and reached similar conclusions.

## 5. Implications for turbulence modelling

The great majority of calculations of turbulent flows use averaged equations which require modelling for closure; for reviews of this subject see Reynolds (1976) and Rodi (1981). In the introduction we noted that none of the presently available turbulence models properly accounts for the effects of rotation.

Since the evidence presented above indicates that the components of the turbulence intensity remain nearly equal when rotation is imposed on isotropic turbulence, there is no need for a model which computes the components of the turbulence intensity. On the other hand, we have found that the lengthscales of the turbulence become anisotropic under the influence of rotation. A model which allows anisotropy of the lengthscales is based on the tensor volume of turbulence (Lin & Wolfstein 1980), but, as W. C. Reynolds (private communication 1981) has shown that some of the quantities in this model may not be finite in all situations, we prefer not to use it. Another model which is based on the integral lengthscales of the turbulence and which allows them to be anisotropic (Donaldson 1973; Sandri & Cerasoli 1981) is currently at an early stage of development. Finally, Reynolds (1982) has proposed a model allowing anisotropic dissipation. As these models are new and not well understood, we shall consider only simple models.

We shall consider a model based on differential equations for the turbulence intensity $Q^2$ and dissipation $\epsilon$; these are related to the lengthscale $l$ by $l = Q^3/\epsilon$, a common assumption in turbulence modelling. The equation for the turbulence intensity is both simple and exact for the flows considered here:

$$\frac{\mathrm{d}Q^2}{\mathrm{d}t} = -2\epsilon, \tag{8}$$

and shows no explicit effects of rotation. Thus any effects of rotation must occur in the dissipation equation. Figure 3 suggests that the effect is approximately linear in the rotation rate, and therefore that the dissipation be modelled by:

$$\frac{\mathrm{d}\epsilon}{\mathrm{d}t} = -c_1 \frac{\epsilon^2}{Q^2} - c_2 \Omega \epsilon, \tag{9}$$

where $\Omega$ is the rotation rate. For more general flows, in which the rotation rate is a function of position or where mean strain may be present, the rotation rate may be locally replaced by $(\Omega_{ij}\Omega_{ij}/2)^{\frac{1}{2}}$, where $\Omega_{ij} = \frac{1}{2}(\partial u_i/\partial x_j - \partial u_j/\partial x_i)$ is the rotation tensor of the mean flow. For $\Omega = 0$, (9) reduces to a commonly used model. The constant $c_1$ is obtained by requiring the model to predict the decay of isotropic turbulence at high Reynolds number; Reynolds (1976) found $c_1 = \frac{11}{3}$. The new term causes the turbulence intensity to decay more slowly as the rate of rotation is increased. For sufficiently high rotation rate and long enough time, the model predicts that the dissipation will go to zero. This is not unreasonable, as these are the conditions under which the flow becomes two-dimensional. In the two-dimensional state, turbulent dissipation will cease and only a small viscous dissipation will remain. A low-Reynolds-number modification may be needed to deal with this situation. Also note that this model may need modification at rotation rates larger than those for which it has been tested. For further comments on this, see Aupoix *et al.* (1983). The system of equations (8) and (9) can be solved analytically:

$$Q^2 = Q_0^2 \left[1 + \frac{2\epsilon_0}{nQ_0}\left(\frac{1 - \mathrm{e}^{-c_2\Omega t}}{c_2\Omega}\right)\right]^{-n}, \tag{10}$$

where

$$n = \frac{2}{c_1 - 2}. \tag{11}$$

This two-equation model was tested against the WN experimental results given in table 3. The constant $c_2$ was obtained by fitting the model to the experimental data of Case B for $\Omega = 80\ \mathrm{s}^{-1}$; we find $c_2 = 0.15$. The initial values of $Q^2$ and $\epsilon$ were obtained from the WN experiment; as noted earlier, they vary with rotation rate.

The two-equation model of (8) and (9) accurately predicts all the WN experimental data on the turbulence intensity. Figure 10 shows the prediction for a case in which the turbulence intensity decays at a slower rate as the rotation rate is increased. Figure 11 shows the prediction of the two-equation model for a case in which the turbulence intensity decays faster at $\Omega = 20\ \mathrm{s}^{-1}$ and slower at $80\ \mathrm{s}^{-1}$; as shown earlier, the faster decay at $\Omega = 20\ \mathrm{s}^{-1}$ is an effect of the initial conditions. Figure 12 shows the prediction of the two-equation model for the WN case used as a test case in the 1980–81 AFOSR Stanford-HTTM Conference on Complex Turbulent Flows. No entry to the conference was able to predict this flow, but the model proposed here has no difficulty with it.

The rotation term in (9) may play an important role in shear flows. Since any shear can be decomposed into plane strain and rotation, it is possible that the new term proposed here will help predict differences between strained and sheared flows; this is a serious deficiency in present models. The model has been used by Mansour, Kim & Moin (1983) who found that addition of the new term in the model improved prediction of the reattachment length for flow over a backward-facing step. However, they found that $c_2 = 0.07$ was required.

Aupoix *et al.* (1983) have studied rotating shear flows with large-eddy simulation and agree that the rotation term in the model is needed. They further suggest that the 'production of dissipation' term (which is zero for the flows considered here) also needs to be modified to account for the effects of rotation.

| | | | |
|---|---|---|---|
| Case A. $M = 0.0039$ m | | | |
| $\Omega$ s$^{-1}$ | 0 | 20 | 80 |
| $U$ m/s | 8.69 | 8.66 | 8.82 |
| $U_s$ m/s | 8.69 | 8.67 | 8.96 |
| $Q^2$ (m$^2$/s$^2$) | 0.2125 | 0.2021 | 0.2314 |
| $\epsilon$ (m$^2$/s$^3$) | 17.67 | 16.45 | 18.19 |
| $Re_T$ | 17–14 | 17–14 | 18–15 |
| $Ro_T$ | $\infty$ | 13.5–1.7 | 3.6–0.6 |
| Case B. $M = 0.00625$ m | | | |
| $\Omega$ s$^{-1}$ | 0 | 20 | 80 |
| $U$ m/s | 5.33 | 5.45 | 5.48 |
| $U_s$ m/s | 5.33 | 5.46 | 5.71 |
| $Q^2$ (m$^2$/s$^2$) | 0.0850 | 0.0906 | 0.0995 |
| $\epsilon$ (m$^2$/s$^3$) | 2.649 | 3.591 | 3.300 |
| $Re$ | 17–15 | 16–14 | 18–16 |
| $Ro$ | $\infty$ | 6.3–1.2 | 1.5–0.4 |
| Case C. $M = 0.00254$ m | | | |
| $\Omega$ s$^{-1}$ | 0 | 20 | 80 |
| $U$ m/s | 8.51 | 8.58 | 8.79 |
| $U_s$ m/s | 8.51 | 8.59 | 8.93 |
| $Q^2$ (m$^2$/s$^2$) | 0.1770 | 0.1774 | 0.1969 |
| $\epsilon$ (m$^2$/s$^3$) | 24.27 | 22.56 | 22.42 |
| $Re$ | 12–9 | 12–10 | 14–11 |
| $Ro$ | $\infty$ | 16–1.2 | 4.0–0.4 |

TABLE 3. Experimental data of Wigeland & Nagib (1978) at initial time ($Ut/M = 20$) and parameter ranges covered

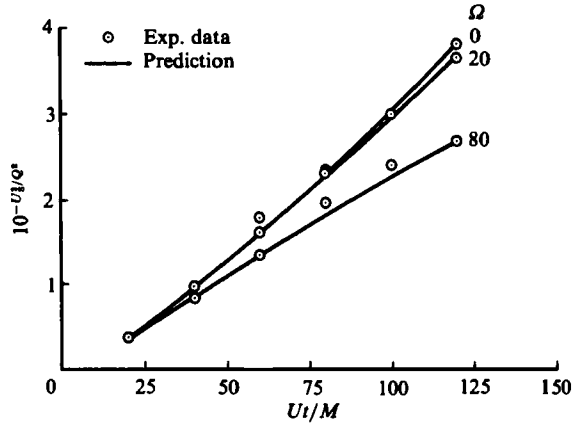


FIGURE 10. Two-equation model prediction of Wigeland & Nagib's (1978) experimental results on the decay of homogeneous rotating turbulence; Case A of table 3.

## 6. Conclusions

We have shown that computer simulation can be used as an aid to understanding the effect of rotation on homogeneous isotropic turbulence. Two effects were found in the experimental results. In the initial region, there is a rotation effect on the generation of the turbulence which increases the initial turbulence intensity and dissipation. Downstream, the primary effect of rotation on the turbulence is a redistribution of energy in wavenumber space, leading to a decrease in the dissipation

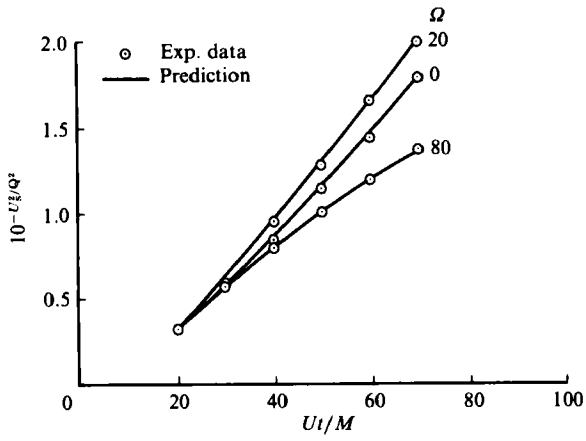


FIGURE 11. Two-equation model prediction for Case B of table 3.

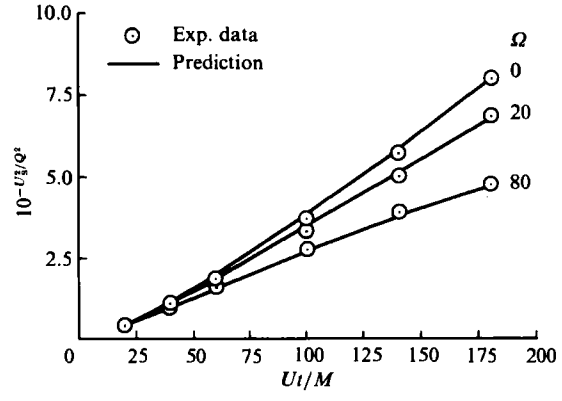


FIGURE 12. Two-equation model prediction for Case C of table 3.

and an increase in the lengthscales, principally those in the direction of the axis of rotation.

The observed effects can be explained in terms of conversion of turbulence energy to inertial waves, resulting in a greatly reduced energy cascade.

Finally, a two-question model has been offered which is capable of reproducing the reduced dissipation in the absence of mean strain.

The Stanford portion of this work was done under grant NCC-2-15, sponsored by NASA-Ames Research Center. The authors wish to acknowledge the contributions to this work made by W. C. Reynolds, M. Rubesin, and P. Moin.

## Appendix. Introduction to large-eddy simulation

In large-eddy simulation, the large eddies are defined by filtering the full velocity field. The filter function utilized is the following Gaussian filter:

$$G(r;\Delta) = \mathrm{e}^{-r^2/6\Delta^2} \tag{A 1}$$

where $\Delta$ is the filter width and the filtered field is mathematically defined as:

$$\bar{u}(\boldsymbol{r},t) = \int G(\boldsymbol{r}-\boldsymbol{r}';\Delta)\,u(\boldsymbol{r}',t)\,\mathrm{d}\boldsymbol{r}'. \tag{A 2}$$

The governing equations of motion of the large eddies are determined by applying the filter function to (2) and (3) of the text. We obtain

$$\frac{\partial \bar{u}_i}{\partial t}+\frac{\partial}{\partial x_j}\overline{\bar{u}_i \bar{u}_j} = 2\epsilon_{ij3}\Omega \bar{u}_j - \frac{1}{\rho}\frac{\partial \bar{p}}{\partial x_i}+\nu\frac{\partial^2 \bar{u}_i}{\partial x_j \partial x_j}+\frac{\partial \tau_{ij}}{\partial x_j}, \tag{A 3}$$

and

$$\frac{\partial \bar{u}_i}{\partial x_i} = 0, \tag{A 4}$$

where

$$\tau_{ij} = \overline{u_i u_j} - \overline{\bar{u}_i \bar{u}_j} \tag{A 5}$$

are the subgrid-scale Reynolds stresses which are modelled by using the Smagorinsky (1963) model:

$$\tau_{ij} = \nu_T\left(\frac{\partial \bar{u}_i}{\partial x_j}+\frac{\partial \bar{u}_j}{\partial x_i}\right) = 2\nu_T \bar{S}_{ij}; \tag{A 6}$$

and

$$\nu_T = (c\Delta)^2 \bar{S}, \tag{A 7}$$

where $\bar{S} = 2(\bar{S}_{ij}\bar{S}_{ij})^{\frac{1}{2}}$ is the strain rate of the large-scale field and $c$ is a constant which can be obtained by any of several methods. The value of the model constant used in this paper is 0.21 and was obtained by fitting the experimental results of Comte-Bellot & Corrsin (1971) on the decay of homogeneous isotropic turbulence.

Since large-eddy simulation provides only the large-scale field, the full turbulence intensity is obtained by using the following equation proposed by Bardina *et al.* (1980, 1983):

$$Q^2 = \frac{\bar{Q}^4}{\bar{Q}^2 - 1.1(2\bar{\epsilon}\Delta)^{\frac{2}{3}}}, \tag{A 8}$$

where $\bar{Q}^2 = \langle \bar{u}_i \bar{u}_i \rangle$ and $\bar{\epsilon} = \langle 2\nu_T \bar{S}_{ij}\bar{S}_{ij} \rangle$ are the turbulence intensity and rate of dissipation of the large eddies, respectively. Equation (A 8) has been successfully tested against experimental results for homogeneous shear flows and isotropic flows.

## REFERENCES


Aupoix, B., Cousteix, J. & Liandrat, J. 1983 Effects of rotation on isotropic turbulence. In *Proc. 4th Symp. Turbulent Shear Flows, Karlsruhe.*

Bardina, J., Ferziger, J. H. & Reynolds, W. C. 1980 Improved subgrid-scale models for large-eddy simulations. *AIAA 13th Fluid and Plasma Dynamics Conf., AIAA Paper* 80-1357.

Bardina, J. Fertiger, J. H. & Reynolds, W. C. 1983 Improved turbulence models based on large eddy simulation of homogeneous, incompressible, turbulent flows. *Rep.* TF-19, *Dept. of Mech. Engng, Stanford University, Stanford, CA.*

Bertoglio, J. P. 1982 Homogeneous turbulent field in a rotating frame. *AIAA J.* **20**, 1175.

Bertoglio, J. P. & Mathieu, J. 1983 Study of subgrid models for sheared turbulence. In *Proc. 4th Symp. Turbulent Shear Flows, Karlsruhe.*

Comte-Bellot, G. & Corrsin, S. 1971 Simple Eulerian time correlation of full- and narrow-band velocity signals in grid-generated 'isotropic' turbulence. *J. Fluid Mech.* **48**, 273–337.

Donaldson, C. du P. 1973 Construction of a dynamic model of the production of atmospheric turbulence and the dispersal of atmospheric pollutants. *Workshop on Micrometeorology* (ed. D. A. Haergen), pp. 313–392. American Meteorological Society, Boston.

Ferziger, J. H. 1981 Higher-level simulations of turbulent flows. *Rep* TF-16 *Dept. of Mech. Engng, Stanford University, Stanford, CA.*

Ferziger, J. H. & Leslie, D. C. 1979 Large eddy simulation – a predictive approach to turbulent flow computation. *AIAA Computational Fluid Dynamics Conf., AIAA paper* 79-1441.

Ferziger, J. H. & Shaanan, S. 1976 Effect of anisotropy and rotation on turbulence production. *Phys. Fluids* **19**, 596–597.

GREENSPAN, H. P. 1968 *The Theory of Rotating Fluids.* Cambridge University Press.

HOPFINGER, E. J. & BROWAND, F. K. 1982 Vortex solitary waves in a rotating turbulent flow. *Nature*, to be published.

HOPFINGER, E. J., BROWAND, F. K. & GAGNE, Y. 1982 Turbulence and waves in a rotating tank, submitted to *J. Fluid Mech.*

IBBETSON, A. & TRITTON, D. J. 1975 Experiments on turbulence in a rotating fluid. *J. Fluid Mech.* **68**, 639–672.

JOHNSTON, J. P., HALLEEN, R. M. & LEZIUS, P. K. 1972 Effects of spanwise rotation on the structure of two-dimensional, fully developed, turbulent channel flow. *J. Fluid Mech.* **56**, 533–557.

KLINE, S. J., CANTWELL, B. J. & LILLEY, G. M. 1982 *1980–81 AFOSR-HTTM-Stanford Conference on Complex Turbulent Flows*, vol. 2, Dept. of Mech. Engng, Stanford University.

LAUNDER, B. E., PRIDDIN, C. H. & SKARMA, B. I. 1977 The calculation of turbulent boundary layers on spinning and curved surfaces. *Trans. ASME* I: *J. Fluids Engng*, 231–239.

LIN, A. & WOLFSTEIN, M. 1980 Tensorial volume of turbulence. *Phys. Fluids* **23**, 644–646.

MANSOUR, N. N., KIM, J. & MOIN, P. 1983 Computation of turbulent flows over a backward-facing step. In *Proc. 4th Symp. Turbulent Shear Flows, Karlsruhe.*

REYNOLDS, W. C. 1976 Computation of turbulent flows. *Ann. Rev. Fluid Mech.* **8**, 183–208.

REYNOLDS, W. C. 1982 Physical and analytical foundations, concepts, and new directions in turbulence modeling and simulation. In *Proc. École d'été d'Analyse Numérique de la Turbulence, Électricité de France*, to appear.

RODI, W. 1979 Influence of buoyancy and rotation on equations for the turbulent lengthscale. In *2nd Intl Symp. Turbulent Shear Flows, London*, pp. 1037–1342.

RODI, W. 1981 Progress in turbulence modeling for incompressible flows. *AIAA 19th Aerospace Sciences Meeting, AIAA Paper* 81-0045.

ROGALLO, R. S. 1981 Numerical experiments in homogeneous turbulence. *NASA* TM-81315.

SANDRI, G. & CERASOLI, C. 1981 Fundamental research in turbulent modeling. Part 1. Theory. Part 2. Experiment. *ARAP Rep. No.* 438. Also published as AFOSR-TR-81-0332, February 1981.

SMAGORINSKY, J. 1963 General circulation experiments with the primitive equations. *Mon. Wea. Rev.* **91**, 99.

TRAUGOTT, S. C. 1958 Influence of solid-body rotation on screen-produced turbulence. *NACA Tech. Note* 4135.

TRITTON, D. J. 1981 Comments on 'Effect of anisotropy and rotation on turbulence production'. *Phys. Fluids* **24**, 1921–1922.

WIGELAND, R. A. & NAGIB, H. M. 1978 Grid-generated turbulence with and without rotation about the streamwise direction. *IIT Fluids and Heat Transfer Rep.* R78-1, Illinois Inst. of Tech., Chicago, Illinois.